BEILSTEIN JOURNAL OF NANOTECHNOLOGY

Free-radical gases on two-dimensional transition-metal disulfides (XS_2, X = Mo/W): robust half-metallicity for efficient nitrogen oxide sensors

Chunmei Zhang, Yalong Jiao, Fengxian Ma, Sri Kasi Matta, Steven Bottle and Aijun Du*

Full Research Paper

Open Access

Address:
School of Chemistry, Physics and Mechanical Engineering, Queensland University of Technology, Gardens Point Campus, QLD 4001, Brisbane, Australia

Email:
Aijun Du* - aijun.du@qut.edu.au

* Corresponding author

Keywords:
free radical; half-metallicity; nitric oxide (NO); sensors; spin-polarized

Beilstein J. Nanotechnol. **2018,** *9,* 1641–1646.
doi:10.3762/bjnano.9.156

Received: 27 November 2017
Accepted: 11 May 2018
Published: 05 June 2018

Associate Editor: N. Motta

Abstract

The detection of single gas molecules is a highly challenging work because it requires sensors with an ultra-high level of sensitivity. By using density functional theory, here we demonstrate that the adsorption of a paramagnetic unpaired free radical gas (NO) on a monolayer of XS_2 (X = Mo, W) can trigger the transition from semiconductor to half metal. More precisely, the single-layer XS_2 (X = Mo, W) with NO adsorbed on it would behave like a metal in one spin channel while acting as a semiconductor in the other spin orientation. The half-metallicity is robust and independent of the NO concentration. In contrast, no half-metallic feature can be observed after the adsorption of other free radical gases such as NO_2. The unique change in electronic properties after the adsorption of NO on transition-metal sulfides highlights an effective strategy to distinguish NO from other gas species by experimentally measuring spin-resolved transmission. Our results also suggest XS_2 (X = Mo, W) nanosheets can act as promising nanoscale NO sensors.

Introduction

Nitrogen oxide (NO_x) gases, one of the most common groups of air pollutants, are known as one culprit of acid rain and can cause serious health issues [1]. For a large-scale monitoring of NO_x, it is highly essential to develop the techniques of toxic gas detection. Up to now, a number of three dimensional (3D) materials, such as nickel phthalocyanine (NiPc) [2], tungsten trioxide (WO_3) [3], mesoporous silicate [4], composites of nanoflower-like Cu_xO and multilayer graphene (CuMGCs) [5] have been successfully synthesized as new types of room-temperature NO gas sensors.

Compared with 3D materials [6], two-dimensional (2D) materials (sheets with thickness of on atom) [7-15] such as graphene [8,16], phosphorene [9], siligraphene (SiC_5) [10] and molybdenum disulfide (MoS_2) [11,17] possess a high specific surface area and high electrical conductivity making them the ideal

candidates for gas sensors. In particular, investigations of XS_2-based (X = Mo, W) monolayer nanodevices demonstrate that they are ultra-sensitive to a number of molecules that are important in environmental studies [18-26]. More specifically, it has been suggested that MoS_2 exhibits ultrahigh sensitivity to the adsorption of paramagnetic gases such as NO and NO_2 [11]. Single-layer MoS_2 has been confirmed to be a good candidate for fabricating field-effect transistor (FET) sensors for NO with high mobility at room temperature [17], and the detection offers a high sensitivity and rapid current response. However, the detailed mechanism regarding the interaction between the MoS_2 surface and the gas molecules remains unclear. In addition to MoS_2, 2D WS_2 is expected to be a more promising material as gas sensor because of its higher thermal stability and wider temperature range of operation [18]. Synthesized FETs layered with WS_2 are also reported as attractive electronic devices [27]. Besides, the corresponding binding position and energy of NO adsorbed on single-layer MoS_2 [23] and WS_2 [28] were analyzed from a theoretical point of view. Even though the gas-sensing properties involving NO and NO_2 are well studied, few studies [29] have been carried out to explore the difference in spin-polarized gas-sensing between NO and other gas molecules.

A completely spin-polarized current flow can be achieved in a half-metallic material [30-33]. Half-metallic materials exhibit semiconducting behavior in one spin channel and metallic behavior in the opposite spin channel, which could be uses in spintronics. But the lack of suitable materials limits the development of spintronic applications. Doping semiconductors may be applied to achieve spin-polarized currents, but this requires a complicated process. Although many materials have been predicted in theory for this purpose, only few possess all necessary properties and many of them are unstable. Therefore, to explore more experimentally feasible and stable half-metallic materials is highly desirable.

In this paper, a density functional theory (DFT) study is carried out to show that monolayer XS_2 (X = Mo, W) can selectively detect NO by exhibiting half-metallicity after physical adsorption of gas on the surface. For comparison, an investigation of NO_2 adsorbed on single-layer XS_2 (X = Mo, W) is also presented as both NO and NO_2 are free radicals and can introduce magnetic moments to the gas/XS_2 (X = Mo, W) system. The binding position and adsorption energy are analyzed in detail. In terms of the projected density of states (PDOS) and orbital contribution, our results offer a deep insight into the Fermi-level pinning mechanism. In addition, we expand the calculations to other 2D layered materials including GaS, GaSe, SnS, SnSe, WSe and Bi_2Se_3 (Figure S1, Supporting Information File 1). To the best of our knowledge, our work is the first to propose a NO sensor by detecting spin transmission, which may probe a new prospect for gas sensing.

Computational Methods

The spin-polarized calculations for NO, NO_2, and NO, NO_2 adsorbed on monolayer XS_2 (X = Mo, W) are performed using DFT within generalized gradient approximation (GGA) of the Perdew–Burke–Ernzerhof (PBE) functional, as implemented in the Vienna ab initio simulation package (VASP) [34-36]. To study 2D systems under the periodic boundary conditions, a vacuum layer with a thickness of more than 20 Å was set to minimize artificial interactions between neighboring layers. A dispersion correction of total energy (DFT-D3 method) [37] is used to incorporate the long-range van der Waals interaction. The structures are fully relaxed until energy and force are converged to 10^{-6} eV and 0.001 eV/Å, respectively. The calculations on band structures and charge density are undertaken with an energy cut-off of 500 eV for the plane-wave expansion and Monkhorst–Pack *k*-point meshes of 3 × 3 × 1 in the whole Brillouin zone. The adsorption energy (binding energy), E_{ads} is calculated according to

$$E_{ads} = E_{tot} - E_{XS_2} - E_{gas}, \quad (1)$$

where E_{tot} is the total energy with adsorbed NO_x after geometry optimization of the adsorbate; E_{gas} is the energy of the adsorbed NO_x molecule after geometry optimization, and E_{XS_2} is the energy of 3 × 3 monolayer XS_2 supercell.

Results and Discussion

We focus our discussions on the adsorption of NO and NO_2 on XS_2 (X = Mo, W), as NO and NO_2 are paramagnetic free radicals. Most other gas molecules, such as NH_3, CO and CO_2, have no magnetic moment. Monolayer XS_2 (X = Mo, W) have a hexagonal configuration, where three pairs of S atoms are anchored on one X atom and form alternating corners (S–X–S) in a honeycomb network. Figure 1 illustrates the top and side view structures of the favorable NO and NO_2 adsorption position on the 3 × 3 supercell of XS_2 (X = Mo, W), and Table 1 summarizes the corresponding values of adsorption energy and magnetic moment. The equilibrium height is defined as the vertical distance between N (NO), O (NO_2) and the top S-layer of the XS_2 (X = Mo, W) sheet (see Figure 1). The calculation based on a 3 × 3 supercell of monolayer XS_2, with a single gas molecule adsorbed on it, is chosen as the computational model. A different gas concentration including the model of a unit cell and 6 × 6 supercell with a single gas molecule adsorbed on the surface are also computed (Figure S2, Supporting Information File 1). In Figure 1, the favorable adsorption configuration for NO is the N atom on top of the X–S bond. N is adjacent to S atoms at the monolayer with a distance of 2.839 and 2.735 Å for

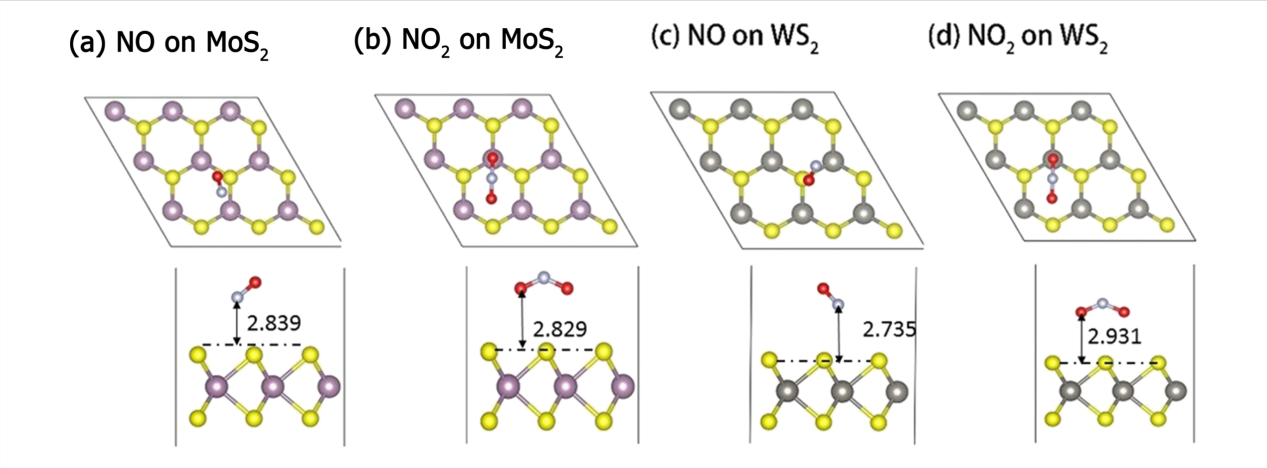

Figure 1: Top and side views of the most favorable NO and NO_2 adsorption configurations on monolayers of MoS_2 and WS_2. The yellow, purple, grey, white and red balls represent S, Mo, W, N, and O atoms, respectively.

Table 1: Calculated values of adsorption energy (E_{ads}) and magnetic moment (M) in equilibrium.

	NO		NO_2	
	E_{ads} (meV)	M (μ_B)	E_{ads} (meV)	M (μ_B)
MoS_2	−180	1	−233	1
WS_2	−165	1	−201	1

single-layer MoS_2 and WS_2, resulting in adsorption energies of −180 and −165 meV (calculated from Equation 1), respectively. NO_2 is bonded with the O atoms close to the monolayer with adsorption distances of 2.829 and 2.931 Å, and adsorption energies of −233 and −201meV, respectively, for single-layer MoS_2 and WS_2 (Figure 1). An adsorption distance of approximately 3 Å suggests that NO and NO_2 are physically adsorbed.

After determining the most favorable adsorption positions, we calculated the electronic properties after the adsorption of NO and NO_2. Both NO and NO_2 are free radical gas molecules with a magnetic moment of 1μ_B. To fully understand the NO_x adsorption mechanism, it is important to understand the interactions between the monolayer and the adsorbate molecules. Investigations [8,28] revealed that charge transfer occurs from the XS_2 (X = Mo, W) nanosheet to the physically adsorbed gas molecules. With the calculated favorable configuration, we compute the corresponding magnetic charge density, total density of state (TDOS) as well as PDOS (Figure S3, Supporting Information File 1) for pristine 2D XS_2 (X = Mo, W) and 2D XS_2 (X = Mo, W) with adsorbed NOx (x = 1, 2; Figure 2). Pristine 2D XS_2 (X = Mo, W) has a band gap of approximately 2 eV. In the case of NO adsorbed on XS_2 (X = Mo, W), a large density of spin-up electrons appear around the Fermi level, while no spin-down electrons appear. Analyzing the PDOS of a

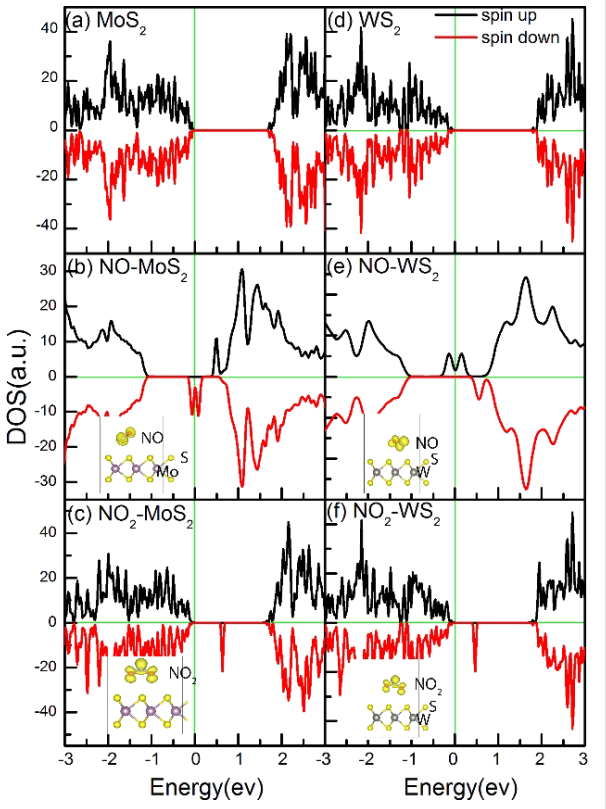

Figure 2: (a–c) TDOS and magnetic charge distribution of (a) the pristine MoS_2 monolayer, and MOS_2 with (b) adsorbed NO and (c) adsorbed NO_2. (d–f) TDOS and magnetic charge distribution of (d) the pristine WS_2 monolayer, and WS_2 with (e) adsorbed NO and (f) adsorbed NO_2. The Fermi level is indicated by the vertical green line.

WS_2 nanosheet with adsorbed NO (Figure S3a–d; Supporting Information File 1), we conclude that the N and O p-orbitals result in absolute spin polarization. In the WS_2 monolayer with adsorbed NO_2, no apparent DOS peaks are present around the

Fermi level (Figure 2f). The spatial magnetic charge distribution analysis suggests that all the spin-unpaired electrons are localized on the NO and NO_2 molecule (insets of Figure 2b,c,e,f) [30].

The concept of Fermi-level pinning is usually used in the metal–semiconductor interface region. Zhou et al. [28] Introduced the concept of Fermi-level pinning into the field of gas/2D nanomaterial systems. However, they failed to point out the spin-polarized Fermi-level pinning in gas/2D nanomaterial system. Based on this, we take the single-layer WS_2 as an example to elucidate the different Fermi-level pinning processes of adsorption of NO and NO_2. The spin orbital-resolved band structures are simulated (Figure 3) and the Fermi level of the adsorbed gas (NO and NO_2)/WS_2 nanomaterial system is pinned around the lowest unoccupied molecular orbital (LUMO) or highest occupied molecular orbital (HOMO) of the adsorbed gas molecules. The PDOS for WS_2 with adsorbed NO indicates that the W and S atoms have no spin polarization (Figure S3c,d; Supporting Information File 1) and the dominant contribution to the HOMO and the LUMO at the Fermi level originates from the p-orbitals of N and O gas atoms (Figure S3a,b; Supporting Information File 1). Therefore, only the p-orbitals of N and O atoms are plotted in Figure 3. For NO adsorption, only the spin-up p-orbitals (red line in Figure 3a) are pinned around the Fermi level, while the spin-down p-orbitals (green line in Figure 3b) are pinned about 0.5 eV above the Fermi level indicating that the electrical current is completely spin-polarized, which is known as half-metallicity. Therefore, the WS_2 monolayer with adsorbed NO is ideal for spintronic applications since it has one metallic spin channel and one semiconducting spin channel. After NO_2 adsorption (Figure 3b), the spin-down and spin-up p-orbitals of the N and O atoms are pinned approximately 0.5 and 2 eV above the Fermi level, respectively. Some impurity states of WS_2 are pinned slightly below the Fermi level upon adsorption of NO_2. These impurity states come from the hybridization of spin-up and spin-down orbitals of the W and S atoms (Figure 3c–e), which contribute to the current flow and fail to enable NO_2/2D WS_2 system display half-metallicity.

In an attempt to address the selectivity towards NO gas in moist environments, we have carried out some new calculations on the adsorption of NO_x (x = 1, 2) on the WS_2 monolayer in the presence of a water molecule. The structures and spin-polarized TDOS for 2D WS_2 with adsorbed NO_x in humid environment are given in Figure S4 (Supporting Information File 1) and Figure 4, respectively. It can be seen that in humid environment, the spin-polarized current is still presented in the WS_2 nanosheet with adsorbed NO (Figure 4b) around the Fermi surface, while no apparent spin-polarized current appears when NO_2 is adsorbed (Figure 4b) or in the pristine WS_2 monolayer (Figure 4a). This shows that the half-metallic property for WS_2 with adsorbed NO can be detected even in a humid environment. The water adsorption energy and distance are around −190 meV and 3 Å, suggesting that water is physically adsorbed on the surface of the WS_2 nanosheet.

Monolayer MoS_2 [38] and multilayer MoS_2 field effect transistors [17] for sensing NO at room temperature have been fabricated experimentally. In this work, the ab initio molecular dynamics simulations at room temperature (300 K) for a 3 × 3 supercell model were performed to further evaluate the thermal stability of MoS_2 with and without the adsorption of NO_x (x = 1, 2) as shown in Figure S5 (Supporting Information File 1). There is no significant structural distortion within 7 ps for the adsorption of NO_x onto MoS_2, indicating highly thermal stability."

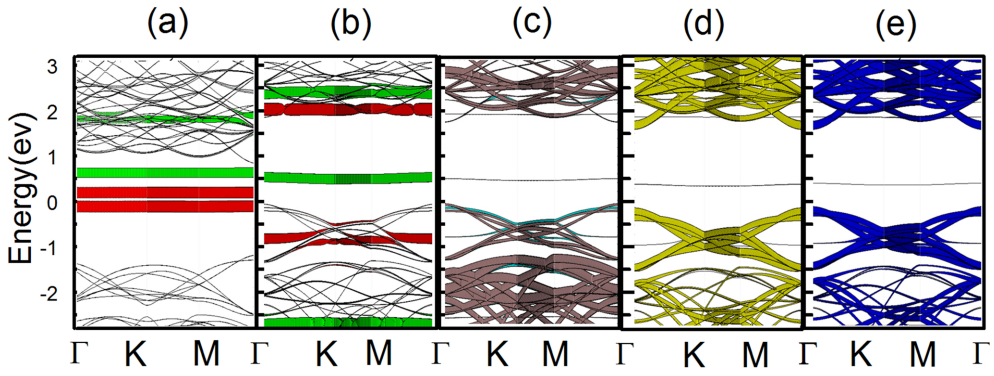

Figure 3: Spin orbital-resolved band structures for WS_2 with (a) adsorbed NO and (b–e) adsorbed NO_2. The red and green lines represent the contributions from the spin-up and spin-down p-orbitals of N and O atoms. Cyan lines and brown lines represent the contributions from the spin-up and spin-down p-orbitals of S atoms. Yellow lines and blue lines represent the contributions from the spin-down and spin-up orbitals of W atoms. The Fermi level is set to the energy zero point.

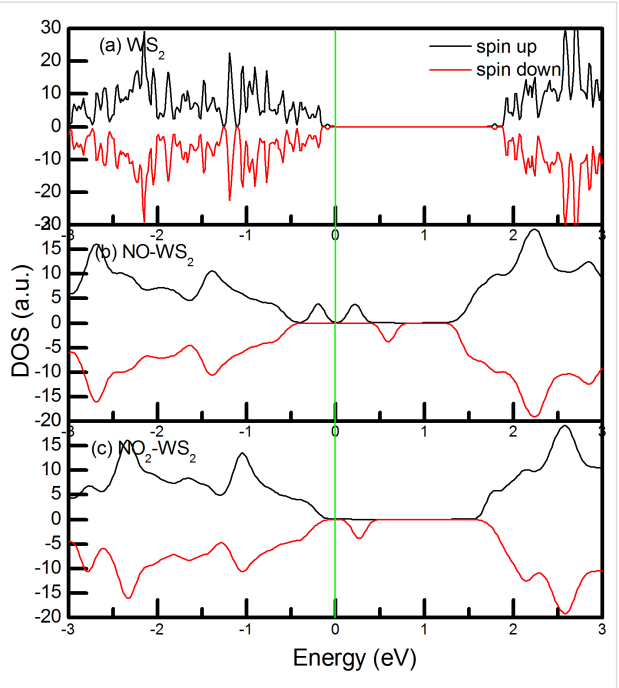

Figure 4: TDOS of (a) the pristine WS_2 monolayer, and the WS_2 monolayer with (b) NO adsorbed and (c) NO_2 adsorbed in humid environment. The Fermi level is indicated by the vertical green line.

Conclusion

We have presented monolayer XS_2 (X = Mo, W) as NO sensor based on first principles studies. The adsorption sites and energy for NO and NO_2 molecules on MoS_2 or WS_2 layers have been studied. The calculations were carried out with different gas concentrations to confirm that the predicted half-metallicity is indeed robust. Differences in electronic properties and orbital analysis between NO and NO_2 adsorption show that half-metallicity is only observed when NO is adsorbed. Since single/multi-layer MoS_2 FET sensors for NO have been experimentally obtained, our strategy to detect gas molecules is promising to be applicable.

Supporting Information

Supporting Information File 1

Additional computational data.
[https://www.beilstein-journals.org/bjnano/content/supplementary/2190-4286-9-156-S1.pdf]

Acknowledgements

We acknowledge generous grants of high-performance computer time from the Computing Facility at the Queensland University of Technology, The Pawsey Supercomputing Centre and Australian National Facility. A.D. greatly appreciates the Australian Research Council QEII Fellowship (DP110101239) and financial support of Australian Research Council under Discovery Project (DP130102420 and DP170103598).

ORCID® iDs

Sri Kasi Matta - https://orcid.org/0000-0003-4465-640X
Aijun Du - https://orcid.org/0000-0002-3369-3283

References

1. Ko, G.; Kim, H.-Y.; Ahn, J.; Park, Y.-M.; Lee, K.-Y.; Kim, J. *Curr. Appl. Phys.* **2010,** *10,* 1002–1004. doi:10.1016/j.cap.2009.12.024
2. Ho, K.-C.; Tsou, Y.-H. *Sens. Actuators, B* **2001,** *77,* 253–259. doi:10.1016/S0925-4005(01)00742-0
3. Zhang, W.; Uchida, H.; Katsube, T.; Nakatsubo, T.; Nishioka, Y. *Sens. Actuators* **1998,** *49,* 58–62. doi:10.1016/S0925-4005(98)00129-4
4. Yamada, T.; Zhou, H.-S.; Uchida, H.; Tomita, M.; Ueno, Y.; Ichino, T.; Honma, I.; Asai, K.; Katsube, T. *Adv. Mater.* **2002,** *14,* 812–815. doi:10.1002/1521-4095(20020605)14:11<812::AID-ADMA812>3.0.CO;2-W
5. Yang, Y.; Tian, C.; Wang, J.; Sun, L.; Shi, K.; Zhou, W.; Fu, H. *Nanoscale* **2014,** *6,* 7369–7378. doi:10.1039/c4nr00196f
6. Yu, F.; Wang, T.; Wen, Z.; Wang, H. *J. Power Sources* **2017,** *364,* 9–15. doi:10.1016/j.jpowsour.2017.08.013
7. Tang, Q.; Zhou, Z.; Chen, Z. *J. Phys. Chem. C* **2012,** *116,* 4119–4125. doi:10.1021/jp211779w
8. Leenaerts, O.; Partoens, B.; Peeters, F. M. *Phys. Rev. B* **2008,** *77,* 125416. doi:10.1103/PhysRevB.77.125416
9. Kou, L.; Frauenheim, T.; Chen, C. *J. Phys. Chem. Lett.* **2014,** *5,* 2675–2681. doi:10.1021/jz501188k
10. Dong, H.; Wang, L.; Zhou, L.; Hou, T.; Li, Y. *Carbon* **2017,** *113,* 114–121. doi:10.1016/j.carbon.2016.11.029
11. Zhao, S.; Xue, J.; Kang, W. *Chem. Phys. Lett.* **2014,** *595–596,* 35–42. doi:10.1016/j.cplett.2014.01.043
12. Liu, H.; Li, X.; Chen, L.; Wang, X.; Pan, H.; Zhang, X.; Zhao, M. *J. Phys. Chem. C* **2016,** *120,* 3846–3852. doi:10.1021/acs.jpcc.5b11699
13. Wu, G.; Yang, M.; Guo, X.; Wang, J. *J. Comput. Chem.* **2012,** *33,* 1854–1861. doi:10.1002/jcc.23017
14. Zhang, C.; Jiao, Y.; Ma, F.; Bottle, S.; Zhao, M.; Chen, Z.; Du, A. *Phys. Chem. Chem. Phys.* **2017,** *19,* 5449–5453. doi:10.1039/C7CP00157F
15. Zhang, C.; Jiao, Y.; He, T.; Ma, F.; Kou, L.; Liao, T.; Bottle, S.; Du, A. *Phys. Chem. Chem. Phys.* **2017,** *19,* 25886–25890. doi:10.1039/C7CP04758D
16. Rigoni, F.; Maiti, R.; Baratto, C.; Donarelli, M.; MacLeod, J.; Gupta, B.; Lyu, M.; Ponzoni, A.; Sberveglieri, G.; Motta, N.; Faglia, G. *Nanotechnology* **2017,** *28,* 414001. doi:10.1088/1361-6528/aa8611
17. Li, H.; Yin, Z.; He, Q.; Li, H.; Huang, X.; Lu, G.; Fam, D. W. H.; Tok, A. I. Y.; Zhang, Q.; Zhang, H. *Small* **2012,** *8,* 63–67. doi:10.1002/smll.201101016
18. Huo, N.; Yang, S.; Wei, Z.; Li, S.-S.; Xia, J.-B.; Li, J. *Sci. Rep.* **2014,** *4,* 5209. doi:10.1038/srep05209
19. Zhang, W.; Huang, J.-K.; Chen, C.-H.; Chang, Y.-H.; Cheng, Y.-J.; Li, L.-J. *Adv. Mater.* **2013,** *25,* 3456–3461. doi:10.1002/adma.201301244
20. Perkins, F. K.; Friedman, A. L.; Cobas, E.; Campbell, P. M.; Jernigan, G. G.; Jonker, B. T. *Nano Lett.* **2013,** *13,* 668–673. doi:10.1021/nl3043079

21. Bryden, J. H. *Acta Crystallogr.* **1962,** *15,* 167–171. doi:10.1107/S0365110X62000407
22. He, Q.; Zeng, Z.; Yin, Z.; Li, H.; Wu, S.; Huang, X.; Zhang, H. *Small* **2012,** *8,* 2994–2999. doi:10.1002/smll.201201224
23. Yue, Q.; Shao, Z.; Chang, S.; Li, J. *Nanoscale Res. Lett.* **2013,** *8,* 425–432. doi:10.1186/1556-276X-8-425
24. Ding, K.; Lin, Y.; Huang, M. *Vacuum* **2016,** *130,* 146–153. doi:10.1016/j.vacuum.2016.05.005
25. O'Brien, M.; Lee, K.; Morrish, R.; Berner, N. C.; McEvoy, N.; Wolden, C. A.; Duesberg, G. S. *Chem. Phys. Lett.* **2014,** *615,* 6–10. doi:10.1016/j.cplett.2014.09.051
26. Bui, V. Q.; Pham, T.-T.; Le, D. A.; Thi, C. M.; Le, H. M. *J. Phys.: Condens. Matter* **2015,** *27,* 305005. doi:10.1088/0953-8984/27/30/305005
27. Sik Hwang, W.; Remskar, M.; Yan, R.; Protasenko, V.; Tahy, K.; Doo Chae, S.; Zhao, P.; Konar, A.; Xing, H.; Seabaugh, A.; Jena, D. *Appl. Phys. Lett.* **2012,** *101,* 013107. doi:10.1063/1.4732522
28. Zhou, C.; Yang, W.; Zhu, H. *J. Chem. Phys.* **2015,** *142,* 214704. doi:10.1063/1.4922049
29. Kou, L.; Du, A.; Chen, C.; Frauenheim, T. *Nanoscale* **2014,** *6,* 5156–5161. doi:10.1039/C3NR06670C
30. Son, Y.-W.; Cohen, M. L.; Louie, S. G. *Nature* **2006,** *444,* 347–349. doi:10.1038/nature05180
31. Qian, M. C.; Fong, C. Y.; Liu, K.; Pickett, W. E.; Pask, J. E.; Yang, L. H. *Phys. Rev. Lett.* **2006,** *96,* 027211. doi:10.1103/PhysRevLett.96.027211
32. Kan, E.-J.; Wu, X.; Li, Z.; Zeng, X. C.; Yang, J.; Hou, J. G. *J. Chem. Phys.* **2008,** *129,* 084712. doi:10.1063/1.2971187
33. Jiao, Y.; Ma, F.; Zhang, C.; Bell, J.; Sanvito, S.; Du, A. *Phys. Rev. Lett.* **2017,** *119,* 016403. doi:10.1103/PhysRevLett.119.016403
34. Kresse, G.; Hafner, J. *Phys. Rev. B* **1993,** *47,* 558–561. doi:10.1103/PhysRevB.47.558
35. Kresse, G.; Furthmüller, J. *Phys. Rev. B* **1996,** *54,* 11169. doi:10.1103/PhysRevB.54.11169
36. Blöchl, P. E. *Phys. Rev. B* **1994,** *50,* 17953. doi:10.1103/PhysRevB.50.17953
37. Grimme, S. *J. Comput. Chem.* **2006,** *27,* 1787–1799. doi:10.1002/jcc.20495
38. He, K.; Poole, C.; Mak, K. F.; Shan, J. *Nano Lett.* **2013,** *13,* 2931–2936. doi:10.1021/nl4013166

License and Terms